Ocean Dynamics (2016) 66:1051–1064
DOI 10.1007/s10236-016-0970-y

Transport of salt and freshwater in the Atlantic Subpolar Gyre

Andreas Born[1,2] · **Thomas F. Stocker**[1,2] · **Anne Britt Sandø**[3,4]

Received: 28 September 2015 / Accepted: 30 June 2016 / Published online: 4 August 2016

Abstract Transport of salt in the Irminger Current, the northern branch of the Atlantic Subpolar Gyre coupling the eastern and western subpolar North Atlantic, plays an important role for climate variability across a wide range of time scales. High-resolution ocean modeling and observations indicate that salinities in the eastern subpolar North Atlantic decrease with enhanced circulation of the North Atlantic subpolar gyre (SPG). This has led to the perception that a stronger SPG also transports less salt westward. In this study, we analyze a regional ocean model and a comprehensive global coupled climate model, and show that a stronger SPG transports more salt in the Irminger Current irrespective of lower salinities in its source region. The additional salt converges in the Labrador Sea and the Irminger Basin by eddy transports, increases surface salinity in the western SPG, and favors more intense deep convection. This is part of a positive feedback mechanism with potentially large implications for climate variability and predictability.

Keywords North Atlantic Ocean · Subpolar Gyre · Irminger current · Climate variability

Responsible Editor: Dieter Wolf-Gladrow

✉ Andreas Born
born@climate.unibe.ch

[1] Climate and Environmental Physics, Physics Institute, University of Bern, Sidlerstrasse 5, 3012 Bern, Switzerland

[2] Oeschger Centre for Climate Change Research, Bern, Switzerland

[3] Institute for Marine Research, Bergen, Norway

[4] Bjerknes Centre for Climate Research, Bergen, Norway

1 Introduction

The Atlantic subpolar gyre (SPG) has repeatedly been identified as one important focal area of decadal variability in the Atlantic Ocean, and a potential source for improved decadal climate predictions (Delworth et al. 1993; Eden and Willebrand 2001; Häkkinen and Rhines 2004; Spall 2008; Yoshimori et al. 2010; Born and Mignot 2012; Robson et al. 2012; Yeager et al. 2012). However, its importance is attributed mostly to the passive advection of surface salinity anomalies of remote origin. The active creation of salinity anomalies by the anomalous SPG circulation itself is rarely considered (Frankignoul et al. 2009).

A strong decline in the SPG circulation strength during the 1990s was first described in observations by Häkkinen and Rhines (2004), who quantified variations with a 'gyre index', the first Empirical Orthogonal Function (EOF) of the satellite altimeter sea surface height. Subsequent work with a regional ocean general circulation model forced by reanalysis data confirmed this finding and associated the weakening of the SPG with a receding subpolar front and high salinities in the eastern subpolar North Atlantic (Hátún et al. 2005b). This westward shift of the subpolar front also corresponds to more surface drifters released in subtropical waters reaching the eastern subpolar North Atlantic (Häkkinen and Rhines 2009).

In the climatological average, relatively saline surface waters of the eastern basin are advected westward by the Irminger Current where they enter the western subpolar North Atlantic. Recent work suggests that when positive salinity anomalies are created in the eastern basin by a weak SPG, they are communicated in the same way (Häkkinen et al. 2011). Paleoclimatic studies extended this concept and concluded that the additional salt transport of a weak SPG enhances Labrador Sea convection and thereby strengthen

the cyclonic circulation through thermal wind (Thornalley et al. 2009). Thus, the SPG would stabilize itself and deep overturning in a negative feedback mechanism. However, this view disregards that the decrease in volume transport counteracts the positive salinity anomaly so that the main source of saline water for the Labrador Sea, salt transport in the Irminger Current, potentially weakens. Thus, without further analysis consequences for the transport of salt and the resulting water mass in the western basin are uncertain.

In this study, we describe how the transport of salt in the Irminger Current decreases with a weaker SPG, as part of a positive feedback mechanism. A stronger circulation also intensifies eddy fluxes, increasing the salinity in the western basin. We employ a simulation of the preindustrial millennium (850 - 1850 AD) with the comprehensive global climate model CCSM4, driven only by external forcing, and a hindcast simulation of the years 1950 - 2002 with a regional version of the ocean model MICOM, constrained by observational hydrography and driven by reanalyzed air-sea fluxes. Both models agree that salt transport in the Irminger Current increases with a stronger SPG, because the increase in volume transport overcompensates lower salinities in its source region. This important role of variations in volume transport was not acknowledged in previous studies although it has important consequences for the stability, variability and thus predictability of the North Atlantic Ocean circulation.

This paper is organized as follows. Section 2 describes the two models used. Section 3 discusses how the SPG changes salt transport and divergence, based mostly on the comprehensive coupled model. Section 4 puts these findings into perspective by comparing it to the regional ocean model and observations. We summarize and conclude in the final Section 5.

2 Description of the models

The simulation results used in this paper are obtained from two general circulation models, the regional Nansen Centre version of the Miami Isopycnal Ocean Model (MICOM) (Sandø and Furevik 2008) and the global coupled Community Climate System Model version 4 (CCSM4; Gent et al. 2011). While the regional model simulates the period from 1950 to 2002 using re-analysis data for atmospheric fluxes and the climatological surface hydrology, the coupled global model is driven only by variations in solar irradiance and volcanic forcing between 850 and 1850 AD.

The regional version of MICOM has a horizontal resolution of approximately 20 km in the region of interest, nested within a global version of the same model with half the resolution (Furevik et al. 2002; Nilsen et al. 2003; Bentsen et al. 2004). Both versions share a vertical resolution of 26 density levels, of which the mixed layer has a variable density and the lower 25 levels vary in thickness defined by fixed isopycnals. The regional refinement covers the Atlantic Ocean between 30° N and 78° N and applies a one-way boundary relaxation scheme toward the global model. Daily mean NCAR/NCEP re-analysis data (Kistler et al. 2001) of fresh water, heat and momentum fluxes are used to force the system by applying the scheme of Bentsen and Drange (2000). In addition, in the regional sub-domain, the mixed layer temperature and salinity fields are linearly relaxed towards the monthly mean climatological values of Levitus and Boyer (1994) and Levitus et al. (1994), respectively. The relaxation time scale adapts to the non-constant thickness of the mixed layer by scaling linearly from 30 days for 50 m thickness to longer times for a thicker mixed layer. The simulation used here is the same as in Hátún et al. (2005a, b), Eldevik et al. (2005), and Mauritzen et al. (2006) and was found to represent hydrological records of the North Atlantic and the southern Nordic Seas realistically. The simulation of the global domain produces climatological averages and variability of the Arctic freshwater and heat transports that generally agree well with observations and an independent high-resolution regional ocean model (Drange et al. 2005).

The ocean component of CCSM4 is a z-coordinate rigid-lid model that employs a curvilinear grid with poles over Antarctica and Greenland (Danabasoglu et al. 2012a). This increases the nominal resolution of 1° to approximately 50 km in the subpolar North Atlantic. The vertical is discretized with 60 levels of uniform 10 m thickness in the upper 160 m and increasing to 250 m at a depth of 3500 m. Several parameterizations of subgrid processes improve the simulation of the subpolar North Atlantic, notably a near-surface eddy flux parameterization (Danabasoglu et al. 2008), a submesoscale mixing parameterization (Fox-Kemper et al. 2008a, b) and an improved representation of density-driven bottom flows across the Greenland-Scotland Ridge (Danabasoglu et al. 2010). The model ocean is coupled without flux adjustments to a finite volume atmosphere model of 1° resolution and 26 vertical levels (Neale et al. 2013) and a comprehensive sea ice model (Hunke and Lipscomb 2008; Holland et al. 2012). In contrast to MICOM, CCSM4 runs freely without relaxation to observed or reconstructed climatological fields. External forcing follows the Paleoclimate Modelling Intercomparison Project Phase III (PMIP3) protocol (Schmidt et al. 2011). The principal changes are variations in total solar irradiance prescribed using reconstructions by Vieira and Solanki (2010) and Lean et al. (2005), and the effect of explosive volcanic eruptions included by an estimate of the stratospheric sulfur aerosol distribution and optical thickness (Gao et al. 2008). A detailed description of this simulation is found in Landrum et al. (2013).

Temperature and salinity of the Labrador Sea, a key region in this study, reproduce observations with good qualitative agreement in both models (Fig. 1). Observations are taken from the World Ocean Atlas 2013, covering the period from 1955 to 2012 (Locarnini et al. 2013; Zweng et al. 2013). Warm saline waters enter the basin on the northern side on the Greenland slope at a depth between 300 m and 1000 m. The temperature of this water mass is about 5 °C in CCSM4 and 3 °C in MICOM. While this is a substantial difference, both values are consistent with the range observed between 1994 and 2005 (Straneo 2006; Yashayaev 2007). Simulated salinities are above 35 psu in CCSM4 and 34.5 psu in MICOM, respectively, which also correspond to the upper and lower extremes in the observations. The very fresh and cold conditions of the Labrador Current, on the southern side of the basin, compare well with observed values, although the location is shifted vertically. The cold water core is found at a depth of 100 m in CCSM4, not at the surface, which could be a result of excessive sea ice in that region (Jahn et al. 2012b). The temperature difference between the models in the warm inflow is also seen in Labrador Sea Water in the central basin between 100 m and 1500–2000 m depth which is warmer than the observed range between 2.7 and 3.5 °C in CCSM4 and about 2 °C colder than that in MICOM. This is density-compensated partly by fresher than observed conditions in MICOM and more saline waters in CCSM4. The bottom of the basin is filled with a relatively cold water mass of 1.5 °C (CCSM4) or 1.2 °C (MICOM) and a salinity of about 34.8 psu, comparable to North East Atlantic Deep Water and Denmark Strait Overflow Water. CCSM4 generally simulates warmer and more saline waters in the Labrador Sea than MICOM.

Both models simulate a seasonal cycle of downward propagating surface temperature anomalies in the Labrador Sea (Fig. 2), indicating that the effect of deep convection is present in the region. The amplitude of temperature variations is similar to observations (Straneo 2006). Comparison to the same observational data set shows that seasonal variations in near-surface salinity are too large in CCSM4. This amplitude is better represented in MICOM. As a result of this difference, deep convection appears to be much shallower in CCSM4 than in MICOM. However, CCSM4 also simulates a stronger vertical temperature gradient that compensates the effect of salinity in terms of density. The Great Salinity Anomaly of the early 1970s is represented in MICOM as a cooling and freshening in the central Labrador Sea, which corresponds well with observations (Dickson et al. 1988; Belkin et al. 1998). Averaged over the study region (black box in Fig. 3), a negligigle linear drift in salinity of -3.3×10^{-4} psu/year (MICOM) and -4.9×10^{-5} psu/year (CCSM4) is observed.

3 Salinity and salt transport in the subpolar gyre

To compare fields of variables associated with differences in the intensity of the SPG, we define a robust metric that has been used in previous model comparisons

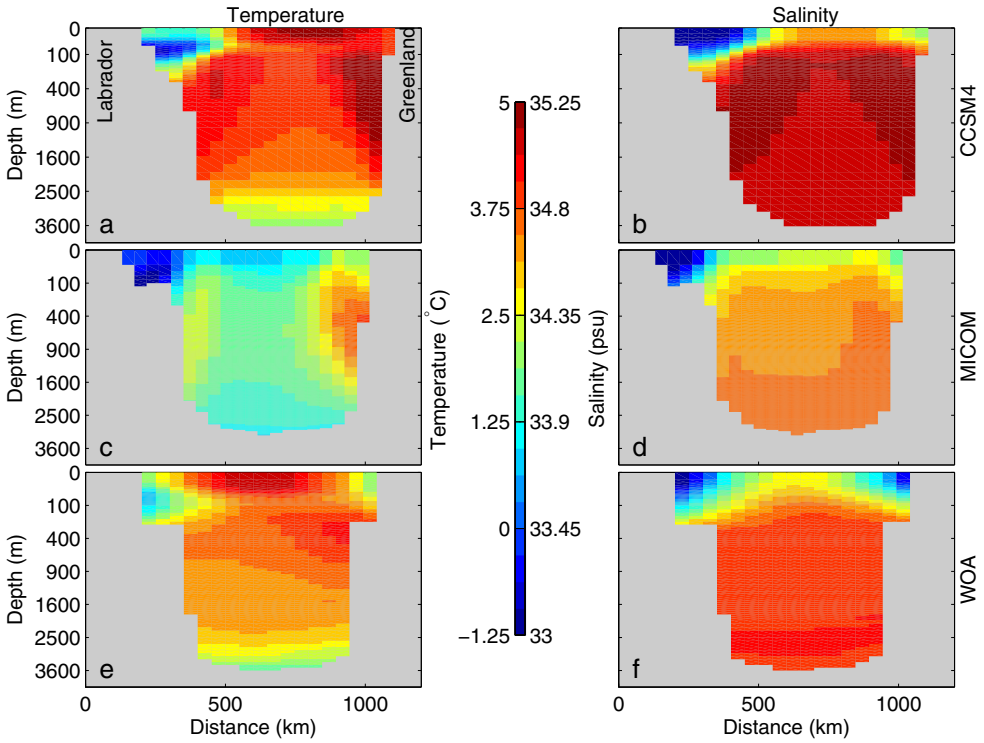

Fig. 1 Temperature (*left*) and salinity (*right*) for CCSM4 (**a**, **b**), MICOM (**c**, **d**), and the World Ocean Atlas (**e**, **f**), for a section through the Labrador Sea (see Fig. 3d), averaged over the entire duration of the simulations, and for 1955–2012 for the WOA

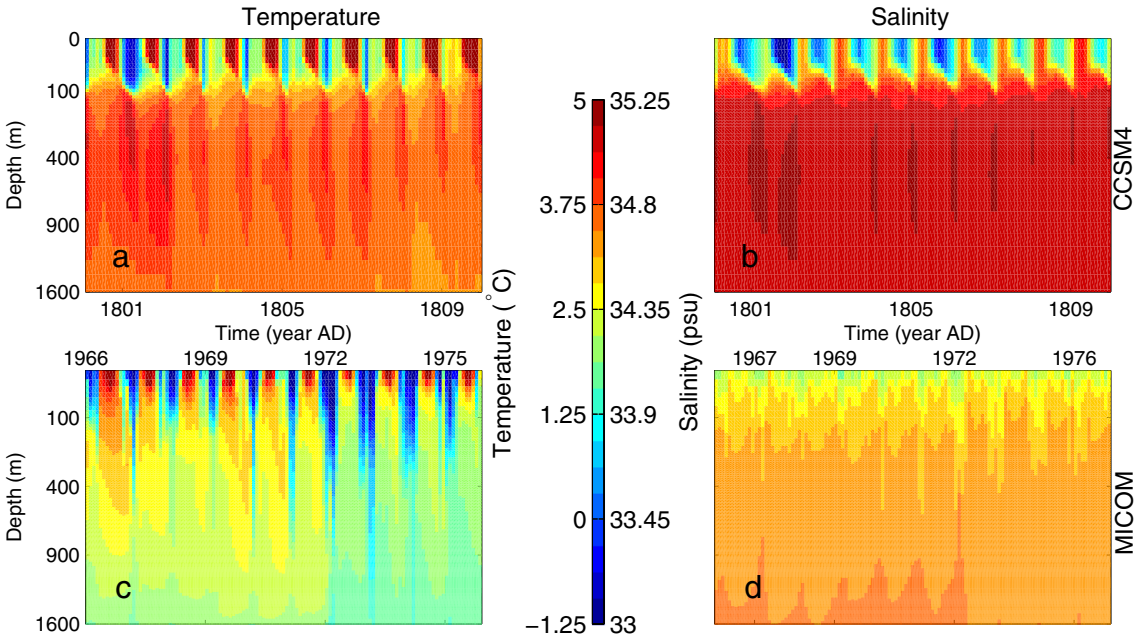

Fig. 2 Hovmöller diagram of temperature (**a**, **c**) and salinity (**b**, **d**) at the central Labrador Sea for CCSM4 (averaged over 10 × 5 grid boxes; **a, b**) and MICOM (averaged over 30 × 15 grid boxes; **c, d**), covering a 10-year time window of monthly data

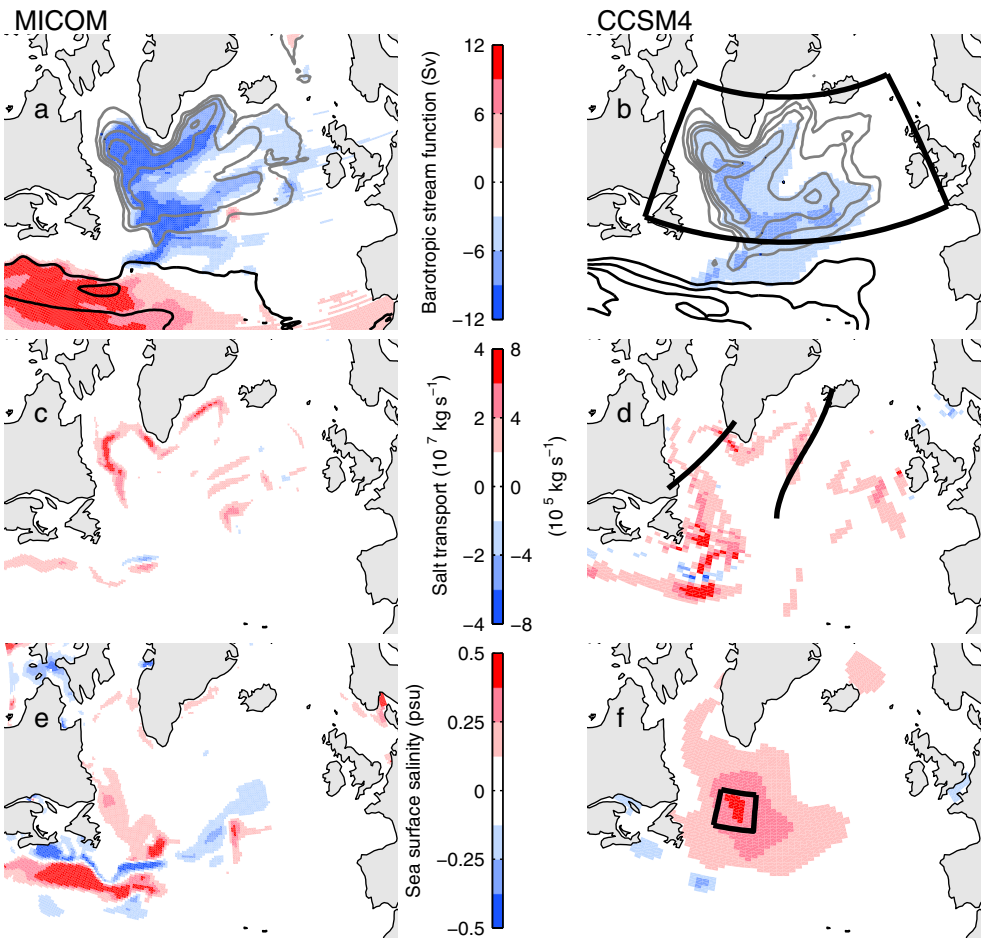

Fig. 3 Composite differences strong–weak SPG_{AVE} for MICOM (*left*) and CCSM4 (*right*); **a, b**: depth-integrated stream function difference (colors). The time-average stream function is shown as a reference (contours, 10 Sv spacing, negative gray, zero omitted); **c, d**: salt transport difference in the mixed layer (MICOM) and the upper 100 m (CCSM4); **e, f:** sea surface salinity difference. The SPG_{AVE} index is defined as the average of the depth-integrated stream function in the black box in **(b)**. The correlation of sea surface salinity inside the *black rectangle* in **(f)** and the SPG_{AVE} index is discussed in the main text. *Black lines* in **(d)** show sections analyzed in Figs. 1 and 4

(Born et al. 2013, 2015). The SPG_{AVE} index is the average of the depth-integrated stream function in the subpolar North Atlantic (60°W–5°W, 48°N–65°N, see Fig. 3b). Composites are defined as exceeding ±1 standard deviation based on annual-average data unless explicitly stated otherwise. Since the stream function is negative for the cyclonic circulation of the SPG, a strong SPG corresponds to a low (negative) SPG_{AVE}.

The time-average circulation of the SPG and patterns of variability are similar in both models. The anomalous circulation is concentrated in the western basin and extends to the south, shifting the North Atlantic Current (Fig. 3a, b). We define the salt transport as $F_S = \sqrt{(u\,S\,\Delta y \Delta z)^2 + (v\,S\,\Delta x \Delta z)^2}$, where S is the local salinity, u and v are the zonal and meridional velocity components, and Δx and Δy the size of one grid box in zonal and meridional direction. In the vertical direction, Δz is 100 m in CCSM4, so that the salinity and the velocities are vertical averages over the upper 10 grid boxes. This depth range covers the active surface layer that most directly impacts deep convection (Fig. 2). For the same reason, Δz covers the uppermost model layer of variable depth in MICOM. Thus, although they agree qualitatively the absolute values of salt transport can not be compared between the two models because the mixed layer is several hundred meters thick in parts of the advection path in MICOM. This problem is not easily amended because the mixed layer is defined very differently in CCSM4 due to the fundamentally different discretization of the vertical model coordinate. Furthermore, one standard deviation of the SPG_{AVE} index, defining the composites in Fig. 3, is more than twice as large in MICOM (1.56 Sv) than it is in CCSM4 (0.76 Sv).

Another consequence of the isopycncal vertical coordinate is that averages over several years potentially combine fields with large differences in layer thickness. As a result, composites in MICOM do not have a well-defined lower boundary in the Cartesian space. On the other hand, a fixed vertical boundary such as that used for the analysis of CCSM4 is not optimal either because isopycnals and thus the interfaces of different water masses are likely to move across it. Such vertical movement could produce a signal that is unrelated to the lateral transport of salt. Notwithstanding the fundamental differences in numerical design and the resulting differences in analysis, both models agree that as a consequence of the enhanced volume transport in the SPG, transport of salt increases around the northern and western rim of the gyre (Fig. 3c, d). This result can thus be considered robust. Extending the depth in CCSM4 to 500 m produces only marginally different results (not shown). Arctic freshwater export, which potentially has a strong impact on the circulation in the North Atlantic (e.g., Kartcher et al. 2005), does not change with variations in the SPG_{AVE} index. Salt transport appears to be more diffuse in CCSM4, partly due to the lower lateral resolution but also because the composites are calculated from 1000 model years with many slightly different looking occurrences of high and low transports.

Sea surface salinities in the western basin increase by up to 0.5 psu with a strong SPG in CCSM4. An increase in salinity is not as clear in MICOM and limited mostly to the boundary currents (Fig. 3e, f). To further test the representativeness of the lower limit of 100 m in CCSM4, the vertical extent of salinity anomalies is analyzed for two representative sections in CCSM4 (Fig. 4). The maximum of the average salinity south of Iceland is found at a depth of 200 to 1000 m, in good agreement with observed hydrography (e.g., Våge et al. 2011). However, salinity anomalies associated with a change in the SPG strength are mostly found in the upper 100 m and barely detectable below 200 m in both sections. In the Labrador Sea, salinity anomalies are most pronounced in the relatively fresh surface layer. Anomalies in the flow, $|u| = \sqrt{u^2 + v^2}$, across the Reykjanes Ridge are also strongest near the surface but can be observed down to a depth of 1000 m. In the Labrador Sea, anomalous velocities also decrease with depth but remain strong almost to the bottom, showing the barotropic nature of the SPG circulation changes.

The anomalous absolute transport of salt can not directly be associated with the changes in surface salinity, because it does not take into account the salinity of the downstream region. However, this first qualitative analysis illustrates that variations in the SPG are associated with more salt transport in the Irminger Current. No consistent changes in the relatively fresh Arctic outflows east and west of Greenland are found with the SPG_{AVE} index.

To quantify how the observed anomaly in surface salinity relates to the anomalous salt transport, we analyze the divergence of the salt transport and its components in CCSM4 (Fig. 5). This type of analysis is not possible in MICOM because of the variable depth of the model layers that would introduce spurious sources and sinks of salt. Note that while this effect is acceptable in the analysis of the absolute transport of salt above it produces a dominant signal in the calculation of spatial derivatives such as the divergence. Interpolation to a grid fixed in space is not possible because the interpolation of the vector field also creates a divergence. As before, the analysis will focus on the upper 100 m where the increase in salinity is most evident and that has the strongest impact on deep convection. However, unlike before, we do not use the volume transport ($u\,\Delta y \Delta z$, $v\,\Delta x \Delta z$) but the vector velocity $\boldsymbol{U} = (u, v)$ because the divergence $\nabla \cdot (S\,\boldsymbol{U})$ yields the readily understandable unit of salinity change per unit time (psu s^{-1}). The results are presented as the difference of the composites $\pm 1\sigma$ of the SPG_{AVE} index.

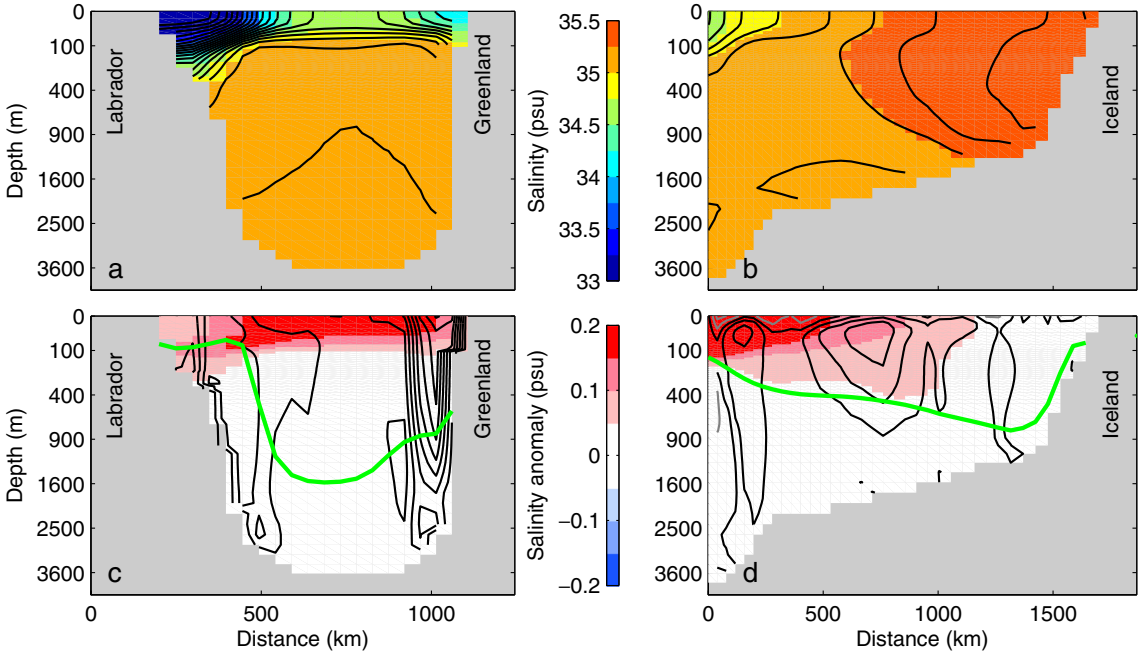

Fig. 4 Average (**a**, **b**) and composite differences SPG_{AVE} strong–weak (**c**, **d**) of salinity in CCSM4 for sections across the Labrador Sea (**a**, **c**) and along the Reykjanes Ridge (**b**, **d**). Anomalous velocities (*black contours*, spacing 0.5 cm s^{-1}, *negative gray*) and average March mixed layer depth (*green contours*) are shown in the *lower panels*. *Black contours* in *upper panels* are isohalines with a spacing of 0.125 psu. Locations of sections shown in Fig. 3d

With a strong SPG, convergence of salt is found primarily around the southern tip of Greenland, while several smaller regions show salinity changes of both signs (Fig. 5a). It is clear that converging salt transport explains only part of the anomaly observed in the salinity field. High salinities appear to mostly result from a stronger doming of isopycnals and therewith enhanced upward mixing of saline water from deeper layers (Fig. 5b). Deeper layers in this region are generally more saline (Figs. 1, 4) and thus a shoaling of the 1028 kg m^{-3} isopycnal, on average located at approximately 500 m depth in CCSM4, brings saline waters upward. This is consistent with the lack of higher surface salinities in the isopycnal model MICOM where shoaling isopycnals make the surface layer thinner but do not change its tracer composition.

The enhanced convergence of the salt transport occurs in a region of deep convection which is thereby enhanced (Fig. 5d). The mixed layer depth increases by approximately 700 m. Stronger deep convection and loss of heat in turn lifts the isopycnals and mixes the more saline subsurface water upward. So, while the observed increase in surface salinity cannot directly be attributed to the convergence of salt at the surface, it is indirectly caused by the enhanced salt transport that strengthens deep convection in the region and thereby mixes more saline waters upward. This is in good agreement with our theoretical understanding of the processes involved (Born and Stocker 2014). Both models agree that these variations in the strength of the SPG do not generally coincide with changes in the East Greenland Current and Arctic freshwater (Fig. 3a–d). Air-sea exchanges play a minor role (Fig. 6). Although the pattern matches the simulated total changes in surface salinity (Figs. 3f, 5b), air-sea freshwater exchange is three orders of magnitude smaller than ocean transports (Fig. 5) and can thus not explain the anomaly. The similarity of the pattern is due to changes in evaporation.

Changes in salt transport depend both on changes in velocity and changes in the salinity of the advected water masses. This is formalized as

$$\begin{aligned}\Delta \boldsymbol{F_S} = \Delta(S \cdot \boldsymbol{U}) &\cong \boldsymbol{U} \cdot \Delta S + S \cdot \Delta \boldsymbol{U} \\ &= \boldsymbol{U} \cdot \Delta S + S \cdot \Delta \boldsymbol{U_{adv}} + S \cdot \Delta \boldsymbol{U_{sg}}, \quad (1)\end{aligned}$$

where the first term $\boldsymbol{U} \cdot \Delta S$ represents changes in salt transport $\Delta \boldsymbol{F_S}$ due to variations in salinity ΔS, scaled by the time-average velocity $\boldsymbol{U}$. The second term $S \cdot \Delta \boldsymbol{U}$ denotes changes in velocity $\Delta \boldsymbol{U}$ scaled by the average salinity S. Terms of higher order ($\Delta S \cdot \Delta \boldsymbol{U}$) are usually small and have been neglected here. The velocity is further divided into its advective component $\boldsymbol{U}_{adv}$ and the parameterized, subgrid part $\boldsymbol{U}_{sg}$, representing mesoscale eddy mixing on isopycnal surfaces following Gent and McWilliams (1990) and the restratification by submesoscale eddies in the mixed layer by Fox-Kemper et al. (2008b).

The divergences of the individual terms in Eq. 1 shows that the divergence of the anomalous transport of salt is almost entirely due to changes in velocity $S\Delta \boldsymbol{U}$ (Fig. 5c).

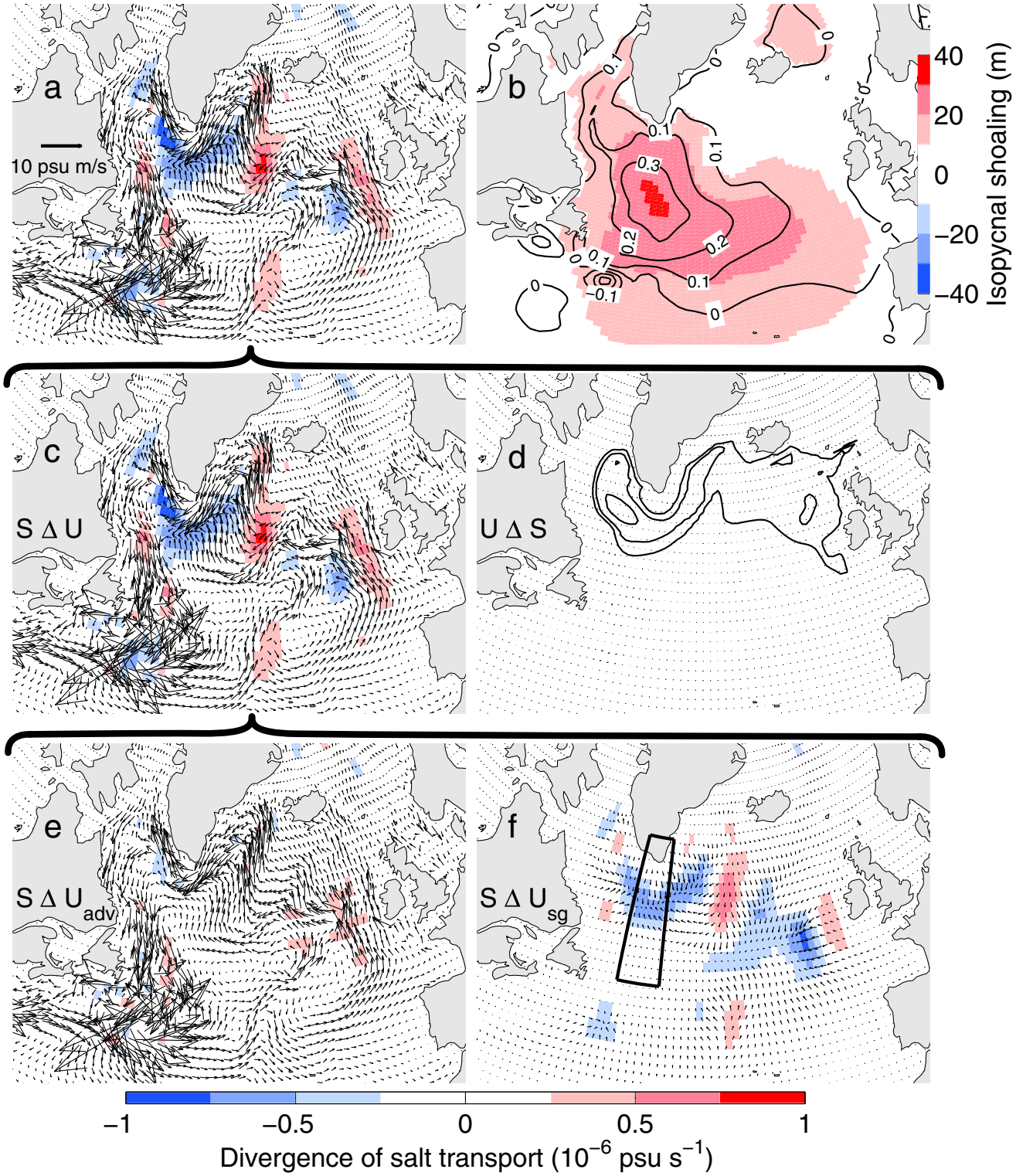

Fig. 5 **a** Composite anomalous salt transport for strong–weak SPG_{AVE} (*arrows*) and divergence thereof (colors) in CCSM4, upper 100 m. **b** Shoaling of the 1028 kg m^{-3} isopycnal (color) and surface salinity anomaly (contours, in psu, see Fig. 3f) for strong–weak SPG_{AVE}. **c, d** As **a**, but only one component of salt transport represents the strong–weak SPG_{AVE} difference, while the other is constant at its climatological average. **e, f** As **c**, decomposed for advective and subgrid flow components. Contours in **d** represent time-average March mixed layer depth (spacing 500 m). Anomalous salt transport is dominated by variations in volume transport ($S\Delta U$) that converge in the deep convection region **(a, c)**. This convergence is mainly due to subgrid (sg) transports **(f)**, while advection transports salt from the eastern to the western basin, but does not converge **(e)**. The *black rectangle* in **(f)** shows the section used in Fig. 7

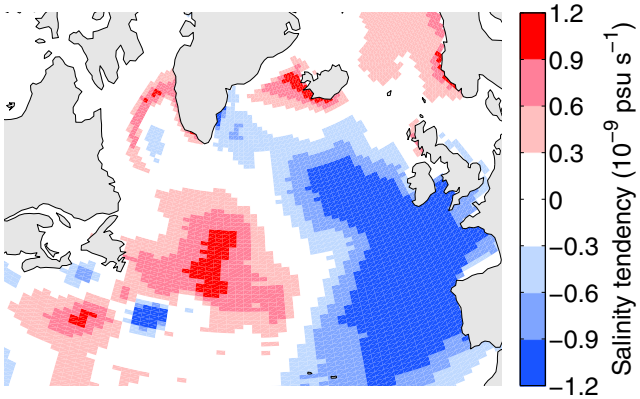

Fig. 6 Tendency of the 100 m averaged salinity due to composited surface freshwater fluxes (evaporation minus precipitation) in CCSM4, strong–weak SPG_{AVE}

Anomalous salinities transported by the climatological flow pattern, $\boldsymbol{U}\Delta S$, do not yield a notable accumulation of salt (Fig. 5d). The decomposition of the velocity into its advective and subgrid components shows that the large-scale transport of salt from the eastern to the western basin is primarily due to advection, while the convergence in the deep convection region is a result of subgrid eddy transports (Fig. 5e, f).

The divergence of salt transport is also calculated in a meridional section through the south of Greenland (Fig. 7). Here, the full three-dimensional fields of salinity and velocity are used. After that, the three-dimensional divergence field is averaged over 5 grid boxes in zonal direction covering the center of the salt convergence (see Fig. 5a, c, f). The convergence of salt transport is most pronounced at the surface where salinity gradients are strongest, but extends down to a depth of about 500 m in the center of the SPG around 56° N. Salt diverges north and south of that, co-located with strong currents perpendicular to the chosen section. This divergence at 53°N and 60°N is partly balancing the convergence in the center of the SPG. The relatively weak divergence is not visible in the horizontal divergence (Fig. 5). At depth, below the region of salt convergence, salt diverges. This picture is consistent with a stronger SPG where eddies transport salt from the relatively saline upper boundary current into the convective center of the SPG and in the opposite direction below (Straneo 2006; Born and Stocker 2014).

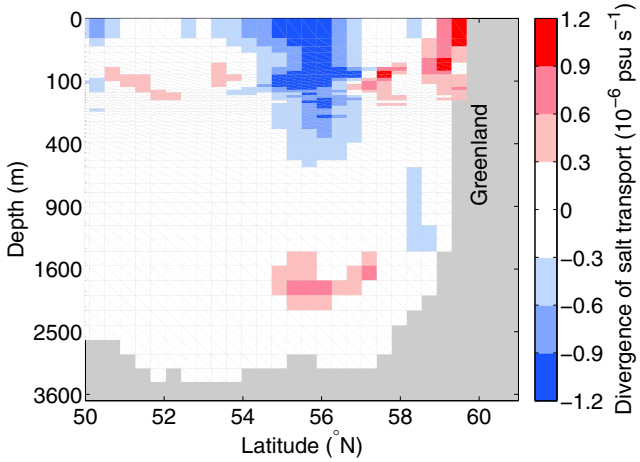

Fig. 7 Divergence of the composite anomalous salt transport for strong–weak SPG_{AVE} in CCSM4. A meridional section is shown extending from southern Greenland following the model grid through the center of the region of maximum convergence (zonal average, see Fig. 5f). Convergence of salt is visible in the center of the SPG around 56° N, coinciding with the horizontal pattern (Fig. 5a)

4 Comparison with MICOM and observations

Since a long integration time is required to obtain robust results for the composites of the divergence, the previous section focusses on the simulation of the last millennium with CCSM4. In the following, we want to take advantage of the good representation of the second half of the last century in MICOM found in previous studies (Hátún et al. 2005a, b) and put some of the above findings into the perspective of recent hydrological changes in the North Atlantic.

Our analysis follows Hátún et al. (2005b) in order to investigate the effect of well-documented hydrographic changes on salt transport and salinity. Therefore, EOFs have been calculated from MICOM sea surface height data of the subpolar North Atlantic to quantify variations in the SPG. Both data and method are identical to the earlier study, but extended in time by using the entire simulation period starting at 1950, ten more years than in Hátún et al. (2005b). This causes minimal changes to the shape of the first two EOFs but inverses their order. The EOF that was dominant for the 1960-2002 period corresponds to the second EOF (EOF2) for the full length of the simulation with 18.9 % explained variance. The first EOF (EOF1) explains 27.3 % of the simulated variance. To visualize the difference, composites of the depth-integrated stream function are defined as greater and smaller than one standard deviation of the time series (principal components, PC) associated with the first two EOFs (Fig. 8). This takes advantage of the complete velocity field simulated by the model without the need to interpret anomalous sea surface height values. The results can directly be compared with the time-average stream function and the composite based on the SPG_{AVE} index in Fig. 3a.

EOF2 does not represent a uniform circulation change in the SPG, but rather a localized recirculation south of Iceland in combination with a relocation of the SPG/STG front. In contrast, the anomalous circulation associated with

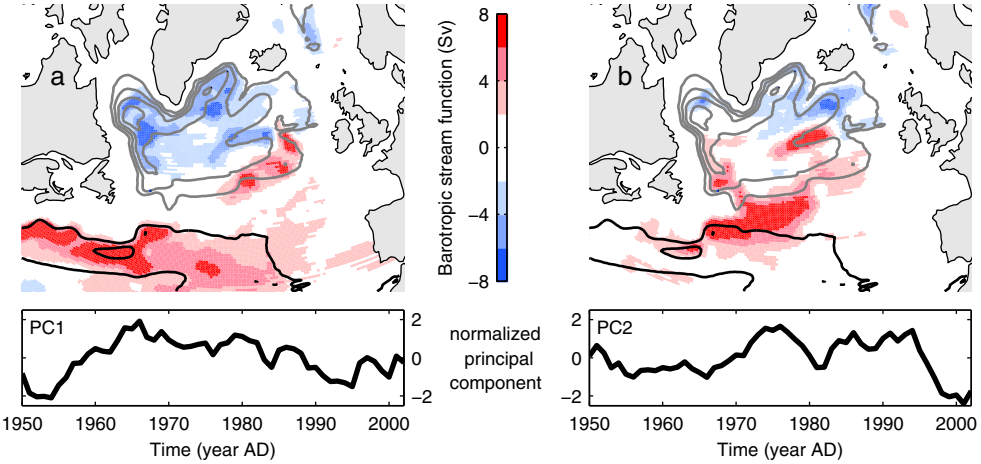

Fig. 8 Composite differences of the depth-integrated stream function of MICOM (colors), based on sea surface height PC1 (**a**) and PC2 (**b**). The normalized PC1 and PC2 are shown in the *lower panels*. Contours show the time-average stream function (spacing 10 Sv, negative gray, zero omitted)

the dominant sea surface height EOF1 appears to be a better representation of variations that involve the entire SPG, including a notable signal in the Labrador Sea (compare Fig. 3a). Interestingly, the anomalous circulation related to EOF1 resembles sea surface height anomalies associated with continuously positive North Atlantic Oscillation index (NAO) forcing in a regional version of the NEMO model, with maxima in the Labrador Sea and the Irminger Basin (Herbaut and Houssais 2009). EOF2 anomalies in MICOM, focused in the northeastern SPG, are not unlike the circulation anomalies caused by continuously positive NAO wind stress forcing (neutral buoyancy fluxes) in NEMO.

Both EOFs are used to calculate composites of salinity and freshwater transport in the subpolar basin, for the variable-depth mixed layer (Fig. 9). The PC2 composite of sea surface salinity, equivalent to the gyre mode of Hátún et al. (2005b), shows the expected freshening south of Iceland with an anomalously positive index (Fig. 9c). It is the result of the relatively small recirculation in the northeastern corner of the SPG (Fig. 8b). A surface freshening is not observed with a more general strengthening of the SPG, the composite of PC1 (Figs. 9a and 3e). Here, salinity anomalies are mostly found in the path of the North Atlantic current but do not propagate into the SPG. Note, however, that the composites are based on relatively short time series and might therefore be contaminated by transient signals such as meanders of the North Atlantic Current.

Anomalies in meridional freshwater transport are calculated as

$$F_y = \iint v \frac{S_0 - S}{S_0}\, dx\, dz, \tag{2}$$

integrated across a section in x direction and over depth z. This is determined for each grid box of the uppermost layer in MICOM individually, with its local salinity S and local meridional velocity v. The reference salinity S_0 is defined as the surface salinity of the western subpolar North Atlantic. The zonal transport of freshwater F_x is calculated analogous to Eq. 2 but using the zonal velocity component u and integrating over y and z.

In the composites based on the PC1 and PC2, most freshwater is transported where the anomalous volume flow is greatest (Figs. 9b, d, and 8). Both composites agree that westward freshwater transport in the Irminger Current decreases with a stronger circulation, irrespective of salinity change in the eastern source region. No noteworthy changes are found outside the SPG, with special attention to freshwater outflow from the Arctic. Waters from the eastern subpolar North Atlantic are generally transported westward in the direction of the Irminger Current and lower salinities are seen along its path in the PC2 composite (Fig. 9c). However, the anomalously low salinity in the eastern basin does not result in an enhanced transport of freshwater toward the west but the causality appears to be opposite. Anomalous freshwater transport is directed toward the east causing the relatively fresh water mass in the eastern SPG. While this appears to contradict the stronger flow of volume, it is indeed a direct consequence. In spite of the decrease in salinity, waters in the eastern basin continue to be more saline than in the western basin. Thus, the additional salt that is transported by the anomalously strong current overcompensates the fact that this water mass is less saline than before, resulting in an overall increased westward transport of salt that is equivalent to a stronger eastward transport of freshwater. This result is consistent with the composites of PC1 that also show a freshwater transport opposite to the direction of the mean flow of volume (Fig. 9b). It also corroborates the analysis of divergence of salt transport in CCSM4 (Fig. 5) and the initial analysis of salt transports (Fig. 3c, d).

The importance for volume flux changes on freshwater transport anomalies in the Irminger Current can be generalized as follows. Meridional Freshwater transport

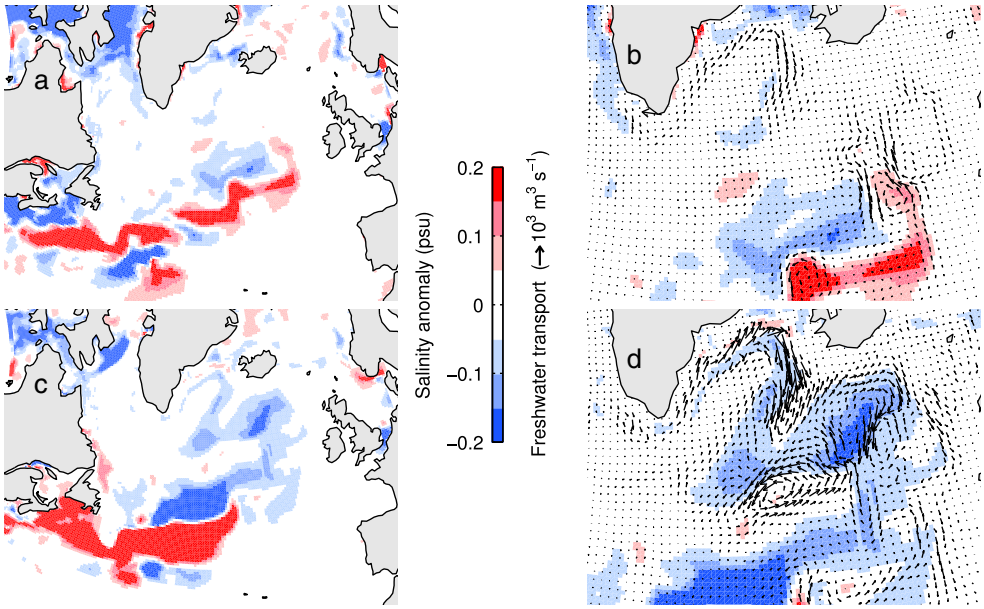

Fig. 9 Composite anomalies of surface salinity (**a, c**) in the uppermost layer in MICOM, based on sea surface height PC1 (*upper*) and PC2 (*lower*). The *right column* shows a closer view of the same salinity data (contours) and *arrows* for freshwater transport for the same composites

across a section of given width and depth is, according to Eq. 2:

$$F_y = V\frac{S_0 - S}{S_0}, \tag{3}$$

where $V = \iint v\,dx\,dz$ is the meridional volume transport. The salinity S is assumed to be constant over the width and depth of the section. Changes in F_y are

$$\Delta F_y = \Delta V \cdot \frac{S_0 - S}{S_0} + V \cdot \Delta\left(\frac{S_0 - S}{S_0}\right) \tag{4}$$

$$= \Delta V \cdot \frac{S_0 - S}{S_0} - \frac{V}{S_0} \cdot \Delta S. \tag{5}$$

We now estimate values for volume transport, salinities and their respective variations from published observations. The average salinity of the Irminger Current is approximately $S = 35$ psu (Våge et al. (2011), Fig. 4), and peak-to-peak interdecadal near-surface variations are smaller than $\Delta S = 0.1$ psu (Hátún et al. 2005b; Häkkinen et al. 2011; Fig. 9). The salinity of the upper central Labrador Sea, taken as the reference salinity S_0 here, is approximately 34.6 psu (Straneo 2006). Estimates of volume transport are less well constrained as they depend on the definition of the Irminger Current by density, salinity or depth contours. To be consistent, the estimates for time-average volume transport and its variations have to represent the water mass corresponding to the observed salinity variations at the near surface. Hence, we employ estimates by Våge et al. (2011) for the northward transport along the western flank of the Reykjanes Ridge, in the upper 500 m: $V = 7$ Sv, $\Delta V = 4$ Sv.

From Eq. 5 the relative magnitude of the freshwater transport contributions from volume flux and salinity variations is:

$$R = \frac{(S_0 - S) \cdot \Delta V}{V \cdot \Delta S} \approx -2.3. \tag{6}$$

Thus, typical variations in volume transport are more than twice as effective in changing the transport of freshwater than accompanying changes in salinity. Moreover, both contributions counteract each other.

The above results from both models and theory indicate that a stronger SPG transports freshwater eastward and concentrates salt in the western basin. However, the strengthening of the SPG from the late 1980s and subsequent weakening after 1995 is not reflected in corresponding salinity changes in observations downstream in the Labrador Sea (Yashayaev 2007), apparently contradicting our findings. The same lack of salinification is observed in the MICOM simulation (Fig. 3). A potential reason why positive salinity anomalies were not observed in spite of the strong SPG before 1995 is that they are relatively small compared to other influences that are not directly associated with the SPG strength such as Arctic freshwater outflows or an accelerated retreat of Greenland outlet glaciers. The observational record that contains only very few variations of the SPG might be too short to reliably separate a salinity anomaly caused by the convergence of the circulation from independent processes. To test this hypothesis, we again use the 1000 year simulation of CCSM4. Sea surface salinity in the western basin (see black rectangle in Fig. 3f) and the (negative) SPG_{AVE} index show a significant (anti-) correlation in this model ($r = -0.5$, Fig. 10).

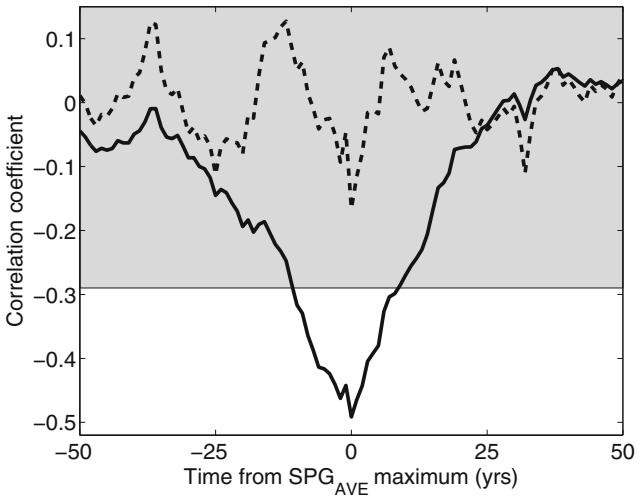

Fig. 10 Cross-correlation of SPG$_{AVE}$ and sea surface salinity in the SPG center (see Fig. 3) for CCSM4, for unfiltered annual data (*solid*) and high-pass filtered data, cut off at a period of 30 years (*dashed*). *Shaded values* are below the significance threshold, for 50 degrees of freedom

To remove information from periods longer than the satellite altimetry record that is commonly used to estimate the SPG circulation strength (∼30 years), both time series are high-pass filtered with a cut-off at 30 years. The resulting cross-correlation is below the 95 % significance threshold ($r = -0.16$) and therefore indistinguishable from a signal of unrelated origin. This suggests that observations of sea surface salinity are too short to discern whether their origin is related to enhanced salt transport and convergence in the SPG. Similar findings have recently been reported from the analysis of five coupled climate models including CCSM4 (Deshayes et al. 2014).

The frequency spectrum of SPG$_{AVE}$ has a significant maximum at 25 years in CCSM4, in agreement with physical explanations described in other coupled models (e.g., Born and Mignot 2012). The significance threshold has been estimated assuming SPG variations of 20 years cycle duration, which gives 50 degrees of freedom for the 1000-year simulation.

5 Summary and conclusions

We investigated the transport and convergence of salt in two general circulation models with very different characteristics, a regional isopycnal ocean model forced by observations for the second half of the last century (1950-2002 AD, MICOM), and a global coupled climate model with a z-coordinate ocean driven by external forcing for the preindustrial millennium (850–1850 AD, CCSM4). While the regional model ensures consistency with recent observations, CCSM4 provides time series long enough for more general and robust conclusions. Indeed, dominant variations in the surface circulation and associated surface salinity fingerprints of recent decades (Hátún et al. 2005b) differ from long-term changes.

Our analysis confirms that a freshening of the eastern basin was the most pronounced water mass change in the 1990s, as a result of an eastward shift of the subpolar front brought about by a recirculation cell in the eastern SPG. For the simulation period of MICOM between 1950 and 2002, this type of circulation anomaly explains a variance in sea surface height of 19 %, the second mode of variability (EOF). However, its spatial pattern does not project onto the time-average barotropic stream function. The association with the SPG is much clearer for the first EOF of sea surface height, explaining 27 % of variance. This latter mode of variability does not show a clear freshening of the eastern basin. We conclude that using the most recent decades of observations as an analogy for past SPG variability might lead to unreliable results (Thornalley et al. 2009).

Both models agree that a stronger SPG transports more salt (less freshwater) along its northern rim as a result of an increased volume transport. Anomalous salinities in the eastern subpolar North Atlantic play a secondary role as the effect of typical changes is smaller than for typical variations in volume transport. This basic result is indeed easily estimated from observational data and is consistent with earlier works that describe the importance of advection for salinity in the Iceland Basin (Herbaut and Houssais 2009) and the Irminger Basin (Desprès et al. 2011).

Transport of salt in the upper layers of the SPG and the connection of the eastern and western subpolar North Atlantic basin have repeatedly been described as important parts of natural climate variability (Delworth et al. 1993; Yoshimori et al. 2010; Lozier 2010; Born and Mignot 2012; Kwon and Frankignoul 2012; Langehaug et al. 2012; Danabasoglu et al. 2012b). Our results suggest that this connection cannot be simplified to the mere communication of existing anomalies from east to west but that the variable transport itself creates substantial salinity anomalies.

The analysis of surface salt convergence adds important detail on the respective roles of explicit advective and parameterized subgrid transports. While advection transports salt over relatively large distances from the eastern into the western basin, it does not converge and therefore not increase the surface salinity in the Labrador Sea. It is the subgrid transports, parameterized eddies, that accumulate salt in the western basin, consistent with observations (Lilly et al. 1999; Lilly and Rhines 2002; Prater 2002; Straneo 2006) and eddy-resolving numerical modeling (Spall 2004). Previous work with CCSM4 found the convergence of subgrid transports to correlate with surface density in the deep convection region, causing changes in the AMOC (Danabasoglu et al. 2012b). We extend these findings and specify that these changes are linked to variations in the SPG and an enhanced advection of salt from east to west.

This understanding supports the concept of the positive feedback mechanism that we presented in previous studies (Born and Stocker 2014; Born et al. 2015): The accumulation of salt in the western basin favors deep convection. Deep convection cools the water column and makes it more dense which strengthens the cyclonic flow of lighter waters around it. This intensification of the SPG then carries more salt again. If less salt was transported in a stronger SPG, e.g., as a result of decreasing salinities in the eastern basin, the feedback would be negative and climate variability of the North Atlantic would arguably be of smaller amplitude (Mengel et al. 2012). This positive advective-convective feedback has been discussed in climate models (Levermann and Born 2007; Born and Mignot 2012; Born et al. 2013) and has successfully been used for the explanation of paleoclimate reconstructions (Born and Levermann 2010; Born et al. 2011; Irvali et al. 2012; Moffa-Sánchez et al. 2014). The good agreement in the time-average circulation and the pattern of variability of the SPG in both models, one of which is designed to resemble the second part of the past century as realistically as possible, suggests that the current generation of coupled climate models simulate this important aspect of climate variability robustly and with reasonable detail.

For the relatively stable climatic periods simulated by the two models used in this study, variations in the SPG do not systematically depend on changes in Arctic freshwater export. Composites based on the strength of the SPG show that the transport of salt within the subpolar North Atlantic dominates over signals from neighboring regions. This situation could change if the Arctic Ocean was affected by an independent forcing. Projected changes in Arctic precipitation, river runoff and sea ice are expected to greatly influence the Arctic outflow of freshwater and thereby the circulation of the North Atlantic (Karcher et al. 2005; Holland et al. 2006; Koenigk et al. 2007; Lehner et al. 2012). This result is robust in spite of the generally poor agreement on the Arctic freshwater budget and exports among coupled climate model (Jahn et al. 2012a). Variations in Arctic sea ice probably also played a decisive role in past climate change (Born et al. 2010; Jochum et al. 2012; Miller et al. 2012; Lehner et al. 2013; Kleppin et al. 2015). However, Born et al. (2010) found that the magnitude of the SPG-internal freshwater flux anomaly is larger than Arctic freshwater fluxes though Denmark Straight for the arguably rather large changes following the last interglacial period 125,000 years ago.

In summary, these findings reinforce the importance of SPG dynamics for large-scale circulation changes. The advection of far-field anomalies into the western subpolar North Atlantic is modified if accompanied by a change in the SPG circulation, which in the case of decadal AMOC variability is observed in virtually all coupled climate models (Yoshimori et al. 2010, Table 1). However, this mechanism does not preclude the modulation by centennial-scale advection of salt anomalies from afar that might be superimposed on the decadal SPG signal (e.g. Delworth and Zeng 2012).

Acknowledgments We gratefully acknowledge comments by Juliette Mignot and three anonymous reviewers. The simulation with CCSM4 was carried out on CISL compute and storage resources. MICOM simulations were supported by the Norwegian Supercomputer Committee. AB was supported by the European Commission under the Marie Curie Intra-European Fellowship ECLIPS (PIEF-GA-2011-300544). TFS acknowledges the support by the Swiss National Science Foundation through grant 159563. ABS was funded by the Norwegian Research Council through projects EPOCASA and NORTH.

References

Belkin IM, Levitus S, Antonov J, Malmberg SA (1998) 'Great salinity anomalies' in the north atlantic. Prog Oceanogr 41:1–68

Bentsen M, Drange H (2000) Parameterizing surface fluxes in ocean models using the NCEP/NCAR reanalysis data. In: Regclim general technical report no 4. Norwegian Institute for Air Research, Kjeller, pp 149–158

Bentsen M, Drange H, Furevik T, Zhou T (2004) Simulated variability of the Atlantic meridional overturning circulation. Clim Dyn 22(6-7):701–720

Born A, Levermann A (2010) The 8.2 ka event: abrupt transition of the subpolar gyre toward a modern North Atlantic circulation. Geochem Geophys Geosyst 11:Q06011

Born A, Mignot J (2012) Dynamics of decadal variability in the Atlantic subpolar gyre: a stochastically forced oscillator. Clim Dyn 39:461–474

Born A, Mignot J, Stocker TF (2015) Multiple equilibria as a possible mechanism for decadal variability in the North Atlantic Ocean. J Clim 28:8907–8922

Born A, Nisancioglu KH, Braconnot P (2010) Sea ice induced changes in ocean circulation during the Eemian. Clim Dyn 35(7):1361–1371

Born A, Nisancioglu KH, Risebrobakken B (2011) Late eemian warming in the nordic seas as seen in proxy data and climate models. Paleoceanography 26:PA2207

Born A, Stocker TF (2014) Two stable equilibria of the Atlantic Subpolar Gyre. J Phys Oceanogr 44:246–264

Born A, Stocker TF, Raible CC, Levermann A (2013) Is the Atlantic subpolar gyre bistable in comprehensive coupled climate models? Clim Dyn 40:2993–3007

Danabasoglu G, Bates S, Briegleb BP, Jayne SR, Jochum M, Large WG, Peacock S, Yeager SG (2012a) The CCSM4 ocean component. J Clim 25:1361–1389

Danabasoglu G, Ferrari R, McWilliams JC (2008) Sensitivity of an ocean general circulation model to a parameterization of near-surface eddy fluxes. J Clim 21:1192–1208

Danabasoglu G, Large WG, Briegleb BP (2010) Climate impacts of parameterized Nordic Sea overflows. J Geophys Res 115:C11005

Danabasoglu G, Yeager SG, Kwon Y-O, Tribbia JJ, Phillips AS, Hurrell JW (2012b) Variability of the atlantic meridional overturning circulation in CCSM4. J Clim 25:5153–5172

Delworth TL, Manabe S, Stouffer RJ (1993) Interdecadal variations of the thermohaline circulation in a coupled Ocean-Atmosphere model. J Clim 6:1993–2011

Delworth TL, Zeng F (2012) Multicentennial variability of the Atlantic meridional overturning circulation and its climatic influence in a 4000 year simulation of the GFDL CM2.1 climate model. Geophys Res Lett 39:L13702

Deshayes J, Curry R, Msadek R (2014) CMIP5 Model intercomparison of freshwater budget and circulation in the north atlantic. J Clim 27(19):3298–3317

Desprès A, Reverdin G, D'Ovidio F (2011) Mechanisms and spatial variability of meso scale frontogenesis in the northwestern subpolar gyre. Ocean Model 39:97–113

Dickson RR, Meincke J, Malmberg S-A, Lee AJ (1988) The "Great salinity anomaly" in the northern north atlantic 1968–1982. Prog Oceanogr 20:103–151

Drange H, Gerdes R, Gao Y, Karcher M, Kauker F, Bentsen M (2005) Ocean general circulation modelling of the nordic seas. In: Drange H, Dokken TM, Furevik T, Gerdes R, Berger W (eds) The nordic seas. An integrated perspective. AGU Geophysical Monograph Series no 158, Washington, DC, pp 199–219

Eden C, Willebrand J (2001) Mechanism of interannual to decadal variability of the north atlantic circulation. J Clim 14: 2266–2280

Eldevik T, Straneo F, Sandø AB, Furevik T (2005) Ventilation and spreading of Greenland sea water. In: Drange H, Dokken TM, Furevik T, Gerdes R, Berger W (eds) The nordic seas. an integrated perspective. AGU Geophysical Monograph Series no. 158, Washington DC, pp 89–103

Fox-Kemper B, Danabasoglu G, Ferrari R, Hallberg RW (2008a) Parameterizing submesoscale physics in global climate models. CLIVAR Exchanges 13:3–5

Fox-Kemper B, Ferrari R, Hallberg R (2008b) Parameterization of mixed layer eddies. Part I: theory and diagnosis. J Phys Oceanogr 38:1145–1165

Frankignoul C, Deshayes J, Curry R (2009) The role of salinity in the decadal variability of the North Atlantic meridional overturning circulation. Clim Dyn 33:777–783

Furevik T, Bentsen M, Drange H, Johannessen JA, Korablev A (2002) Temporal and spatial variability of the sea surface salinity in the Nordic Seas. J Geophys Res 107(C12):8009

Gao C, Robock A, Ammann C (2008) Volcanic forcing of climate over the last 1500 years: an improved ice-core based index for climate models. J Geophys Res 113:D2311

Gent PR, Danabasoglu G, Donner L, Holland M, Hunke E, Jayne S, Lawrence D, Neale R, Rasch P, Vertenstein M, Worley P, Yang Z-L, Zhang M (2011) The community climate system model version 4. J Clim 24:4973–4991

Gent PR, McWilliams JC (1990) Isopycnal mixing in ocean circulation models. J Phys Oceanogr 20:150–155

Häkkinen S, Rhines PB (2004) Decline of subpolar North Atlantic circulation during the 1990s. Science 304:555–559

Häkkinen S, Rhines PB (2009) Shifting surface currents in the northern North Atlantic Ocean. J Geophys Res 114:C04005

Häkkinen S, Rhines PB, Worthen DL (2011) Warm and saline events embedded in the meridional circulation of the northern North Atlantic. J Geophys Res 116:C03006

Hátún H, Sandø AB, Drange H, Bentsen M (2005a) Seasonal to decadal temperature variations in the faroe-shetland inflow waters. In: Drange H, Dokken TM, Furevik T, Gerdes R, Berger WH (eds) The nordic seas. An integrated perspective. AGU Geophysical Monograph Series no 158, Washington DC, pp 239–250

Hátún H, Sandø AB, Drange H, Hansen B, Valdimarsson H (2005b) Influence of the atlantic subpolar gyre on the thermohaline circulation. Science 309:1841–1844

Herbaut C, Houssais M-N (2009) Response of the eastern North Atlantic subpolar gyre to the North Atlantic Oscillation. Geophys Res Lett 36:L17607

Holland MM, Bailey DA, Briegleb BP, Light B, Hunke E (2012) Improved sea ice shortwave radiation physics in CCSM4: the impact of melt ponds and aerosols on arctic sea ice. J Clim 25:1413–1430

Holland MM, Finnis J, Serrenze MC (2006) Simulated arctic ocean freshwater budgets in the twentieth and twenty-first centuries. J Clim 19:6221–6242

Hunke EC, Lipscomb WH (2008) CICE: the los alamos sea ice model user's manual, version 4. Technical report, los alamos national laboratory tech. Report LA-CC-06-012

Irvali N, Ninneman US, Galaasen EV, Rosenthal Y, Kroon D, Oppo DW, Kleiven HF, Darling KF, Kissel C (2012) Rapid switches in subpolar north atlantic hydrography and climate during the last interglacial (MIS 5e). Paleoceanography 27:PA2207

Jahn A, Aksenov Y, de Cuevas B, de Steur L, Häkkinen S, Hansen E, Herbaut C, Houssais M, Karcher M, Kauker F, Lique C, Nguyen A, Pemberton P, Worthen D, Zhang J (2012a) Arctic ocean freshwater: how robust are model simulations? J Geophys Res 117:C00D16

Jahn A, Sterling K, Holland MM, Kay JE, Maslanik JA, Bitz CM, Bailey DA, Stroeve J, Hunke EC, Lipscomb WH, Pollak DA (2012b) Late-twentieth-century simulation of arctic sea ice and ocean properties in the CCSM4. J Clim 25:1431–1452

Jochum M, Jahn A, Peacock S, Bailey DA, Fasullo JT, Kay J, Levis S, Otto-Bliesner B (2012) True to Milankovitch: glacial inception in the new community climate system model. J Clim 25:2226–2239

Karcher M, Gerdes R, Kauker F, Köberle C, Yashayaev I (2005) Arctic ocean change heralds North Atlantic freshening. Geophys Res Lett 32:L21606

Kistler R, Kalnay E, Collins W, Saha S, White G, Wollen J, Chelliah M, Ebisuzaki W, Kanamitsu M, Kousky V, den Dool HV, Jenne R, Fiorini M (2001) The NCEP-NCAR 50-year reanalysis, monthly means, CD-ROM and documentation. Bull Am Meteorol Soc 82:247–268

Kleppin H, Jochum M, Otto-Bliesner B, Shields CA, Yeager S (2015) Stochastic atmospheric forcing as a cause of Greenland climate transitions. 28:7741–7763

Koenigk T, Mikolajewicz U, Haak H, Jungclaus J (2007) Arctic freshwater export in the 20th and 21st centuries. J Geophys Res 112:G04S41

Kwon Y-O, Frankignoul C (2012) Stochastically-driven multidecadal variability of the Atlantic meridional overturning circulation in CCSM3. Clim Dyn 38:859–876

Landrum L, Otto-Bliesner BL, Conley A, Lawrence P, Rosenbloom N, Teng H (2013) Last millennium climate and its variability in CCSM4. J Clim 26:1085–1111

Langehaug H, Medhaug I, Eldevik T, Otterå OH (2012) Arctic/atlantic exchanges via the subpolar gyre. J Clim 25:2421–2439

Lean J, Rottman G, Harder J, Kopp G (2005) SORCE Contributions to new understanding of global change and solar variability. Solar Phys 230:27–53

Lehner F, Born A, Raible CC, Stocker TF (2013) Amplified inception of European little ice age by sea ice-ocean-atmosphere feedbacks. J Clim 26:7586–7602

Lehner F, Raible CC, Hofer D, Stocker TF (2012) The freshwater balance of polar regions in transient simulations from 1500 to 2100 AD using a comprehensive coupled climate model. Clim Dyn 39:347–363

Levermann A, Born A (2007) Bistability of the Atlantic subpolar gyre in a coarse-resolution model. Geophys Res Lett 34:L24605

Levitus S, Boyer T (1994) World ocean atlas 1994 volume 4: temperature. Technical report

Levitus S, Burgett R, Boyer TP (1994) World ocean atlas 1994 volume 3: salinity. Technical report

Lilly JM, Rhines PB (2002) Coherent eddies in the labrador sea observed from a mooring. J Phys Oceanogr 32:585–598

Lilly JM, Rhines PB, Visbeck M, Davis R, Lazier JRN, Schott F, Farmer D (1999) Observing deep convection in the labrador sea during winter 1994/95. J Phys Oceanogr 29:2065–2098

Locarnini R, Mishonov A, Antonov J, Boyer T, Garcia H, Baranova O, Zweng M, Paver C, Reagan J, Johnson D, Hamilton M, Seidov D (2013) World ocean atlas 2013, volume 1: temperature. Technical report

Lozier S (2010) Deconstructing the conveyor belt. Science 328:1507–1511

Mauritzen C, Hjøllo SS, Sandø AB (2006) Passive tracers and active dynamics: A model study of hydrography and circulation in the northern North Atlantic. J Geophys Res 111:C08014

Mengel M, Levermann A, Schleussner C, Born A (2012) Enhanced Atlantic subpolar gyre variability through baroclinic threshold in a coarse resolution model. Earth Syst Dyn 3:189–197

Miller GH, Geirsdóttir A, Zhong Y, Larsen DJ, Otto-Bliesner BL, Holland MM, Bailey DA, Refsnider KA, Lehman SJ, Southon JR, Anderson C, Björnsson H, Thordarson T (2012) Abrupt onset of the little ice age triggered by volcanism and sustained by sea-ice/ocean feedbacks. Geophys Res Lett 39:L02708

Moffa-Sánchez P., Born A, Hall IR, Thornalley DJR, Barker S (2014) Solar forcing of North Atlantic surface temperature and salinity over the past millennium. Nat Geosci 7:275–278

Neale RB, Richter J, Park S, Lauritzen PH, Vavrus SJ, Rasch PJ, Zhang M (2013) The mean climate of the community atmosphere model (CAM4) in forced SST and fully coupled experiments. J Clim 26:5150–5168

Nilsen JE, Gao Y, Drange H, Furevik T, Bentsen M (2003) Simulated North Atlantic-Nordic Seas water mass exchanges in an isopycnic coordinate OGCM. Geophys Res Lett 30:1536

Prater MD (2002) Eddies in the labrador sea as observed by profiling RAFOS floats and remote sensing. J Phys Oceanogr 32:411–427

Robson J, Sutton R, Lohmann K, Smith D, Palmer MD (2012) Causes of the rapid warming of the North Atlantic ocean in the mid 1990s. J Clim 25:4116–4134

Sandø AB, Furevik T (2008) Relation between the wind stress curl in the North Atlantic and the Atlantic inflow to the Nordic Seas. J Geophys Res 113:C06028

Schmidt GA, Jungclaus JH, Ammann CM, Bard E, Braconnot P, Crowley TJ, Delaygue G, Joos F, Krivova NA, Muscheler R, Otto-Bliesner BL, Pongratz J, Shindell DT, Solanki SK, Steinhilber F, Vieira LEA (2011) Climate forcing reconstructions for use in PMIP simulations of the last millennium (v1.0). Geosci Model Dev 4:33–45

Spall MA (2004) Boundary currents and watermass transformation in marginal seas. J Phys Oceanogr 34:1197–1213

Spall MA (2008) Low-frequency interaction between horizontal and overturning gyres in the ocean. Geophys Res Lett 35:L18614

Straneo F (2006) Heat and freshwater transport through the central labrador sea. J Phys Oceanogr 36:606–628

Thornalley DJR, Elderfield H, McCave IN (2009) Holocene oscillations in temperature and salinity of the surface North Atlantic. Nature 457:711–714

Våge K, Pickart RS, Sarafanov A, Knutsen Ø, Mercier H, Lherminier P, van Aken HM, Meincke J, Quadfasel D, Bacon S (2011) The Irminger Gyre: circulation, convection, and interannual variability. Deep-Sea Res I Oceanogr Res Pap 58(5):590–614

Vieira LEA, Solanki SK (2010) Evolution of the solar magnetic flux on time scales of years to millenia. Astron Astrophys 509:A100

Yashayaev I (2007) Hydrographic changes in the Labrador Sea, 1960–2005. Prog Oceanogr 73:242–276

Yeager S, Karspeck A, Danabasoglu G, Tribbia J, Teng H (2012) A Decadal prediction case study: late 20th century North Atlantic Ocean heat content. J Clim 25:5173–5189

Yoshimori M, Raible CC, Stocker TF, Renold M (2010) Simulated decadal oscillations of the Atlantic meridional overturning circulation in a cold climate state. Clim Dyn 34:101–121

Zweng M, Reagan J, Antonov J, Locarnini R, Mishonov A, Boyer T, Garcia H, Baranova O, Johnson D, Seidov D, Biddle M (2013) World ocean atlas 2013, volume 2: salinity. Technical report